

A comparative first-principles investigation on the defect chemistry of TiO₂ anatase.

Marco Arrigoni* and Georg K. H. Madsen

Institute of Materials Chemistry, TU Wien, A-1060 Vienna, Austria

(Dated: April 9, 2024)

Abstract

Understanding native point defects is fundamental in order to comprehend the properties of TiO₂ anatase in technological applications. Several first-principles studies have been performed in order to investigate the defect chemistry of this material. The reported values are, however, scattered over a wide range. In this manuscript we perform a comparative study employing different approaches based on semilocal, DFT+ U and screened hybrid functionals in order to investigate the dependence of defect properties, such as formation energies and charge transition levels, on the employed computational method. While the defects in anatase, like in most transition-metal oxides, generally induce the localization of electrons or holes on atomic sites, we notice that, provided an alignment of the valence bands has been performed, the calculated defect formation energies and transition levels using semi-local functionals are in a fair agreement with those obtained using hybrid functionals. A similar conclusion can be reached for the thermochemistry of the Ti-O system and the limit values of the elemental chemical potentials. We interpret this as a cancellation of error between the self-interaction error and the overbinding of the O₂ molecule in semi-local functionals. Inclusion of a U term in the electron Hamiltonian offers a convenient way for obtaining more precise geometric and electronic configurations of the defective systems.

* marco.arrigoni@tuwien.ac.at

I. INTRODUCTION

TiO₂ is one of the most representative materials in photocatalysis [1, 2], with the anatase polymorph being the most commonly found in synthesized nanoparticles where it shows a higher photocatalytic activity than the thermodynamical stable rutile bulk phase [3, 4]. Anatase is also attracting interest as a promising and inexpensive transparent conducting oxide due to its wide band gap (around 3.2 eV [5]) and large intrinsic *n*-type carrier concentrations [6]. The conductivity decreases after annealing in ambient atmosphere at high temperature [6], but can be further enhanced through doping with group-V elements [7, 8]. TiO₂ is often produced in a reduced state, where it shows states in the gap and a pale-blue color [9]. The non-stoichiometry of reduced TiO₂ has been associated to both oxygen vacancies, titanium interstitials and surface hydroxyl groups [10, 11].

In order to explain the observed features, several first-principles studies have considered the various intrinsic defects of anatase. They tend to agree on the fact that the most relevant electron donors, which govern the *n*-type behaviour of intrinsic anatase, are oxygen vacancies (\square_{O}) and titanium interstitials (Ti_i) and the most important electron acceptor are the titanium vacancies (\square_{Ti}). However, one finds that the values of important quantities, such as defect formation energies and thermodynamic charge transition levels, are very scattered. To emphasize this, we mention how the description of Ti_i and \square_{O} defects may be different both quantitatively and qualitatively. Na-Phattalung *et al.* employed the local density approximation (LDA) and predicted that both Ti_i and \square_{O} are very shallow donors[12]. On the contrary Osorio-Guillén *et al.*, using a generalized gradient approximation (GGA) functional, found that Ti_i and \square_{O} behave like deep donors with transition levels more than 1 eV below the conduction band minimum (CBM) [13]. Morgan and Watson used the GGA+*U* method and also found Ti_i and \square_{O} to be deep donors [14]. Most recently, Boonchum *et al.*[15] and Deak *et al.*[16] used the same screened hybrid functional (HSE06 [17]) to study Ti_i and \square_{O} . While Boonchum *et al.* found \square_{O} to be a very shallow donor and Ti_i to have transition levels located no further than 0.4 eV below the CBM, than Deak *et al.* found transitions between +2/+1/0 charge states of \square_{O} to be 0.4 eV and 0.05 eV below the CBM and +4/+3/+2/0 transition levels for Ti_i to be in the range between 1.3 eV and 0.3 eV below the CBM[16].

Such discrepancies are problematic if one aims to predict the properties of technologically relevant materials by means of first-principles simulations. They are, however, not completely unexpected as the above-mentioned studies employ very different computational methods, involving

not only different exchange-correlation (xc) functionals, but also different correction schemes for charged defects, supercell sizes and pseudopotentials.

Regarding the choice of the xc functional, it is well known that common local and semi-local functionals suffer from two main shortcomings affecting the description of point defects in semiconductor materials [18, 19]. The self-interaction error, due to which portions of the charge density associated with a given electron tend to repel themselves, yields electronic configurations with an exaggerated electron delocalization for those defects which induce localized defective states. Furthermore, the underestimation of the fundamental gap results in a tendency to mix the defect-induced states with the band edges, yielding an erroneous delocalization of the defect-induced charge density in valence-band-like or conduction-band-like states.

Both these shortcomings can be traced to a derivative discontinuity of the exact Kohn-Sham xc functional at integer particle numbers which cannot be reproduced within the LDA and GGAs[20]. To ameliorate them, different approaches have been proposed. Nowadays, hybrid functionals are considered as the method of choice for the first-principle study of point defects in solids since the incorporation the exact exchange partly corrects the self-interaction and introduces an approximated derivative discontinuity for the xc energy. As a consequence, localized states can be described more accurately and the predicted band gap is much closer to the experimental value. In particular, screened hybrid functionals are currently preferred for solids due to their superior accuracy and reduced computational costs with respect to non-screened hybrids [21].

While hybrid functionals seem a suitable choice for the description of point defects, the computational costs involved are still high. The problem is particularly significant for the study of defects, since these require relatively large supercells and non-trivial structure relaxations that can be difficult to explore systematically. A good compromise between computational costs and reliability might be offered by the DFT+ U approach, which aims at a correct description of the derivative discontinuity by the introduction of an on-site U term for localized electrons[22].

Calculated defect energies are influenced by other factors than the xc functional. As mentioned already, even the two studies employing the same hybrid functional reached different conclusions [15, 16]. It would thus be important to isolate the role of the chosen xc functional, the most important approximation present in the Kohn-Sham scheme, from other computational parameters in predicting the properties of point defects in an technologically relevant materials such as TiO₂ anatase. Recently, it has been shown, for certain materials and localized defects, that a good agreement between the the thermodynamic charge transition levels predicted by semi-local and

hybrids functionals can be obtained if the values of the electron chemical potentials are given with respect to a common reference [23–27].

In the present study, we thus investigate the defect chemistry of intrinsic anatase employing different functionals at the semi-local, DFT+ U and hybrid level. By comparing the results, we estimate the level of agreement between different xc functionals. We find that although PBE+ U gives an electronic and geometric structure in better agreement with HSE15, predicted charge transition levels and defect formation energies are in better agreement between semilocal and HSE15 functionals. It thus appears that while PBE+ U would be very useful to estimate the geometric and electronic structure of the defect, which can be used as a starting point for more accurate theoretical approaches, standard GGA functionals are more suitable for a first estimation of the energetic properties of the defect.

II. COMPUTATIONAL METHOD

A. Defect Formation in the Dilute Limit

For the formation of point defects the most appropriate thermodynamic potential is the grand potential [28]. Therefore it is natural to define the defect energy, $\Delta E_d(D^{(q)})$, of a given point defect D in the charge state q as the change in grand potential after the introduction of the defect in the pristine host material:

$$\Delta E_d(D^{(q)}) = \Delta E_f(D^{(q)}) - \sum_i n_i \Delta \mu_i + q \mu_e. \quad (1)$$

where $\Delta E_f(D^{(q)}) = E(D^{(q)}) - E_{\text{bulk}} - \sum_i n_i E_i$ is the defect formation energy with respect to the reference states of the parent elements. $E(D^{(q)})$ is the free energy of the supercell containing the point defect, E_{bulk} is the free energy of the supercell describing the pristine material, n_i is the number of atoms of type i which need to be removed ($n_i < 0$) or added ($n_i > 0$) to the system in order to create the point defect and E_i the energy of the standard state. $\Delta \mu_i$ is the change in chemical potential of the element i from the standard state and μ_e is the chemical potential of the electron. As a common approximation, we replace the Gibbs free energy of the solid with the ground-state electronic energy computed by first-principles. Even though both harmonic[29–31] and anharmonic[32] contributions can have a non-negligible effect on the bulk energies, these are mainly relevant at high temperatures.

The $E(D^{(q)})$ must be corrected for the finite-size-errors which arise in the supercell method

[33]. While most of the errors can be minimized by using a large enough supercell, in the presence of charged defects, electrostatic interactions are too long-ranged and cannot be neglected for any realistic supercell size. Among the various methods proposed in the literature for correcting the electrostatic finite-size effects, we employ the one proposed by Kumagai and Oba, which has proved to be very effective for anisotropic systems and for ionic materials, where large atomic relaxations induced by the presence of a point-defect make the use of other potential alignment methods difficult [34].

A thermodynamic charge transition level is defined as the value that the electron chemical potential must have in order for two different charge states, q and q' , of a defect to have the same defect energy. It is customary to express the electron chemical potential in terms of the valence band maximum of the host material, ε_V , and the Fermi level, E_F , which varies between zero and the band gap of the material: $\mu_e = \varepsilon_V + E_F$. With this convention and using equation (1), we can write the charge transition levels as:

$$\varepsilon_0(q/q') = \frac{E(D^{(q)}) - E(D^{(q')})}{q' - q} - \varepsilon_V, \quad (2)$$

This expression emphasizes how the charge transition levels do not depend on the chemical potentials of the elements but only on the valence band maximum eigenvalue.

B. Chemical Potentials

The values of $\Delta\mu_i$ are important, not only because they enter in equations (1), but also because they give a connection between the first-principles defect calculations and the experimental growth conditions of the system.

Thermodynamic equilibrium constraints the possible values the chemical potentials of the elements can assume. For TiO_2 anatase the constraints are given by the following conditions:

$$\Delta\mu_{\text{Ti}} + 2\Delta\mu_{\text{O}} = \Delta h_f(\text{TiO}_2; \text{anatase}), \quad (3a)$$

$$x\Delta\mu_{\text{Ti}} + y\Delta\mu_{\text{O}} \leq \Delta h_f(\text{Ti}_x\text{O}_y), \quad (3b)$$

$$\Delta\mu_{\text{Ti}} \leq 0, \quad \Delta\mu_{\text{O}} \leq 0 \quad (3c)$$

For Ti we took as standard state the HCP titanium structure and for O we took as the gas phase of the O_2 molecule in its triplet ground state. Δh_f is the enthalpy of formation (per formula unit) of the compound of interest. Equation (3a) represents the thermodynamic stability condition

for TiO_2 anatase and shows that only one of the elemental chemical potential is an independent variable. Equations (3b) and (3c) state the fact that we consider only those thermodynamical states where anatase is stable. Note that while at standard pressure and temperature the thermodynamical stable phase of TiO_2 is rutile, this is not the case within the GGA, GGA+ U and hybrid functionals approximations, as it is shown in section III D. An accurate evaluation of the formation enthalpies of the various oxides is critical for the determination of the chemical potential of Ti. We will discuss these points for the Ti-O system in section III D.

C. Computational Details

We performed the first-principles calculations employing different xc functionals. A series of calculations was done employing the version of the PBE functional revised for solids (PBEsol) [35] while other two series employed the DFT+ U formalism in its rotationally invariant fully localized limit [22, 36]. Finally, for the most relevant electron donor and acceptors, *i.e.* Ti_i and \square_{O} and \square_{Ti} , respectively, we also employed the HSE functional. Since the standard HF admixture of 25% overestimates the band gap by around 0.5 eV, we employed a value of 15% which predicts a band gap of 3.12 eV, in good agreement with the experimental value of around 3.2 eV. In the text, such a parametrization of the HSE functional is denoted as HSE15.

The first batch of DFT+ U series employs the PBE functional and a value of U equal to 5.8 eV which is applied on the 3d states of all Ti atoms of the titanium oxides (except on TiO which is metallic). We denote such approach as PBE+ $U[\text{Ti}]$. The value of U was chosen because it offers a compromise between accurately described cell parameters and the band gap (see Table I). This value is also the value found for d orbitals in TiO from constrained DFT calculations [37]. The second batch of DFT+ U calculations also adds a U term on the 2p O orbitals for the same oxides (PBE+ $U[\text{Ti},\text{O}]$). This was proposed by Morgan and Watson to be necessary in order to correctly describe ionized acceptors such as \square_{Ti} [14]. For the oxygen 2p orbitals we use the same value of U of 5.25 eV proposed by these authors.

All calculations were performed using the projector augmented-wave method [38] as implemented in the computer code VASP [39]. As valence electrons, we considered the 3p, 3d and 4s ones for Ti and the 2s and 2p ones for O. Plane waves up to an energy cutoff of 500 eV were included in the basis set. The calculations on the conventional cell of TiO_2 anatase employed a $6 \times 6 \times 2$ Γ -centered grid for reciprocal space integration. We checked the convergence of the

internal energy up to a large $16 \times 16 \times 8$ Γ -centered grid and found a difference of less than 2 meV per atom. Since the valence band maximum of anatase does not lie at any high-symmetry point in reciprocal space, to obtain an accurate estimation of this eigenvalue we calculated the band structure of the primitive cell. For calculations involving other phases in the Ti-O system, we used a Γ -centered grid with at least $1000/n$ k -points, where n is the number of atoms in the simulation cell. Ionic positions and cell parameters of the pristine systems were optimized until forces on all atoms were below 0.01 eV/Å. The convergence threshold for the electronic energy was set to 10^{-5} eV. Spin polarization was allowed in all calculations.

The dielectric tensor, both ionic and electronic contributions, necessary in order to calculate E_{corr} of equation (1), were calculated using density functional perturbation theory [40, 41] using a dense $24 \times 24 \times 8$ Γ -centered k -point grid. For HSE15 the experimental value has been used.

Point defects were modeled employing a $3 \times 3 \times 1$ expansion of the conventional tetragonal anatase cell. Such supercells contain 108 atoms. The number of k points for reciprocal space integration was reduced accordingly, except for the HSE15 calculations, where due to high computational costs, we employed a Γ -only grid. Ionic positions were optimized using a conjugated-gradient method keeping the same thresholds for forces and total energies as for the pristine systems. The cell parameters were kept fixed to the ground-state values obtained for the pristine system using the corresponding xc functional.

A quite used practice consists in fixing the cell parameters of defective supercells to experimental values or to values obtained from different functionals. This practice is quite common, for example, when as a starting point for more expensive approaches (*e.g.* hybrid functionals) one takes the structures optimized with less time consuming functionals. In practice such an approach induces a pressure on the simulation cell, which can be considerable if we consider the fact that different functionals can disagree on the cell parameters by around 2-3%. To assess the validity of such methods, we calculated the formation energies of point defects in the PBE+ U [Ti] setup both fixing the cell parameters to the ground-state PBE+ U [Ti] values and to the PBEsol values, which are very close to the experimental ones.

In order to compare charge transition levels calculated using different xc functionals, we align the top of the valence bands predicted by the different functionals to the vacuum level by calculating ionization potentials (IPs). To perform such an alignment we use the three-step approach proposed in reference 42. Such approach requires the calculation of the valence-band-maximum eigenvalue, ε_V , in the bulk system and the calculation of the averaged electrostatic potential in the

vacuum region and in a bulk-like region of a sufficient thick slab. We perform slab calculations for the PBEsol, PBE+ U [Ti], PBE+ U [Ti,O] and HSE15 functionals using a 10-atomic-layers slab presenting the non-polar (101) surface of anatase, which is the most stable one [9]. Slabs are separated by their periodic images along the direction perpendicular to the surface by 50 Å of vacuum. Ionic positions were not relaxed as relaxation effects are generally small [43]. Using slabs, and assuming that the surface charge densities are described in a similar way by different functionals and surface dipoles are small, it is possible to reference ϵ_V to the vacuum level by comparing the value of the electrostatic potential obtained in a region far from the surface, which represents the vacuum, to the averaged electrostatic potential in the bulk-like region of the slab. Such procedure gives the IP as predicted by a given functional. Once IPs have been calculated for each xc functional, they can be compared in order to align the obtained valence band maxima to an unique reference, which we take as ϵ_V of the hybrid functional, since hybrids give much more reliable IPs than standard semi-local functionals [44]. The alignment is then given by: $\Delta\epsilon_V = \text{IP} - \text{IP}(\text{Hyb.})$. Where IP(Hyb.) indicates the ionization potential calculated with the hybrid functional HSE15.

III. RESULTS

A. Bulk Properties

TiO₂ anatase crystallizes in a body-centered tetragonal unit cell (space group $I4_1/amd$) containing 12 atoms. The top of the valence band is mainly formed by overlapping oxygen 2*p* orbitals, while the bottom of the conduction band mostly by titanium 3*d* orbitals. Various properties of bulk anatase, calculated with different functionals, are summarized in Table I.

PBEsol and HSE15 give cell parameters in very good agreement with the experimental values, but HSE15 slightly overestimates *c* by 1%. PBE+ U overestimation is larger: the cell parameter *a* is overestimated by around the 2.4% in PBE+ U [Ti] and the 1.8% in PBE+ U [Ti,O]; while the *c* parameter is overestimated by around 2.4% and 2.1%, respectively. The PBEsol band gap is severely underestimated by 35%, as it is expected for semilocal functionals. Both PBE+ U [Ti] and PBE+ U [Ti,O] give a value closer to the experimental one (smaller than \approx 13% and 8%, respectively). The effect of an U term on the Kohn-Sham effective potential is to introduce a repulsive term for less than half-filled states and an attractive one for the other ones[22, 47]. Therefore, adding U to the empty Ti-3*d* states pushes the conduction band maximum up, opening the Kohn-

Sham gap; adding an U term also on the occupied O-2 p states will push the valence band down, opening the gap even more. This fact can also be noticed by considering the last row of Table I which shows that PBE+ U [Ti,O] valence band maximum lies indeed lower than the PBE+ U [Ti] one. Note that for this material the standard parametrization of HSE06 overestimates the band gap by around 17% [15]. The IP calculated for the (101) surface of anatase, using the HSE15 functional, has a value of 7.67 eV, in close agreement with the value predicted for this surface by taking into account many-body effects at the GW level [42], indicating that HSE15 offers a good reference for comparing valence band maxima.

Regarding the computed dielectric tensor, the electronic contribution calculated with PBE+ U [Ti] and PBE+ U [Ti,O] agrees well with the experimental values; while PBEsol tends to overestimate it by an average of the 18%. On the other hand PBE+ U severely underestimate the ionic contribution, while PBEsol gives values in better agreement with the experiments. The values of the dielectric tensor are needed only for correcting the electrostatic finite-size-effects in supercell calculations in the correction scheme of Kumagai and Oba [34]. Therefore, the computed value is the correct one to be used, since it describes consistently with the employed xc functional the medium response to the electric field generated by the array of charged defects, modeled as point charges.

B. Defect Chemistry

In our comparative study we take into account a wide range of point defects and charge states and compare the results keeping the same computational parameters, except for the xc functional (and k -point mesh for hybrid functional calculations), in order to assess the dependency of the calculated values on the choice of the xc functional itself. We considered the largest number of defects within the PBE+ U [Ti] scheme. In particular, we studied: Ti_i as an intrinsic donor in charge states 0, +1, +2, +3, +4. The defect was placed in an interstitial site where it obtained a quasi-pyramidal coordination [48] and occupies the 8e Wyckoff site. \square_{Ti} was considered as an acceptor in the charge states 0, -1, -2, -3, -4, its Wyckoff site is 4a. O_i was studied in the -2, -1, 0, +1, +2 charge states. O_i gives rise to a O_2 dimer whose bond length depends on the charge state [49]. Its center of mass occupies the 8e Wyckoff position. \square_{O} (Wyckoff site 8e) was studied in the donor charge states 0, +1, +2. Several configurations with similar energies have been predicted for this defect [50]. Here we consider the split-vacancy configuration [14] which should represent the

ground state. We also considered the antisites O_{Ti} as donors in charge states 0, -1, -2, -3, -4 and the antisites Ti_{O} as acceptors in charge states 0, +1, +2, +3, +4. Antisites were scarcely studied in the literature, we only found them considered in the study of Ref. 12. As their geometric structure has been barely considered before, we report it here for completeness. These defects originally occupy the same Wyckoff positions of the atoms they substitute. However, we found that for both antisite defects, the antisite atom relaxes along the c direction from the ideal position of the atom it substitutes. Relaxation effects are particularly important for the Ti_{O} defect, due to the large radius of Ti atoms compared to the O one. Ti_{O} defects can be thought as a complex formed by a \square_{O} and a Ti_i . Such findings are summarized in Figure 1. Due to the large strain induced on the host material, such defects have a large formation energy and therefore a minor role in the defect chemistry of anatase.

The problem of localization of excess electrons in anatase has been discussed thoroughly in the literature due to the relevance of electron self-trapping for photocatalytic applications (see for example Ref. 11 and references therein). It has been shown that the nature of these excess electrons is highly affected by the choice of the employed theoretical approach [52]. In particular, employing the $\text{DFT}+U$ approach yields a different description of excess electron localization when different values of U are employed [53]. We calculated self-trapped electrons with the $\text{PBE}+U[\text{Ti}]$ method and we found that it forms a small polaron with a formation energy (the polaron formation energy is defined as $E_{\text{pol}} = E_{\text{loc}}(N+1) - E_{\text{deloc}}(N+1)$, where N is the number of electrons in the pristine system, loc and deloc denote electronic configuration in which the excess electron is localized on a Ti atom or delocalized in a conduction-band-like state, respectively) of around -0.3 eV, in agreement with the study of Setvin *et al.* that found small polarons are stabilized in anatase when a U value larger than 5 eV is used [53]. We also found that the small polaron has a large formation energy, as given by equation (1), of around 3.70 eV; therefore self-trapping appears unlikely for any value of the electron chemical potential within the experimental band gap. Since experimental observations also suggest that excess electrons in anatase are not trapped unless other defects are present [53], we did not consider such species further.

The type of point defect studied with each computational approach is summarized in Table II. For all approaches we considered the most important defects: Ti_i , \square_{O} and \square_{Ti} which are usually studied in the literature. The former two are expected to be the most important electron donors; while the latter the most important electron acceptor. Defects with higher formation energies, like O_{Ti} and Ti_{O} and the small polaron were considered only within the $\text{PBE}+U[\text{Ti}]$ approach.

C. Transition levels

As they are not affected by the chemical potentials of O and Ti, we start our discussion with the comparison of the thermodynamic charge transition levels, $\epsilon(q/q')$, among the different functionals. They are however affected by the predicted value of the valence band maximum, equation (2), which must be aligned with respect to a common reference. This is illustrated in Figure 2 for the most relevant point defects in anatase: Ti_i , \square_{O} and \square_{Ti} , for which we calculated all the charge states for all four computational approaches. In Table III we report the values of $\epsilon(q/q')$ predicted with the employed computational schemes, after having aligned the valence bands with the one predicted by HSE15 calculations.

One can notice that, transition levels can have different qualitative behavior between functionals. The best agreement is obtained between PBE+ U [Ti] and PBE+ U [Ti,O], with a mean absolute error (MAE) of 0.14 eV. This should not be surprising as the inclusion of the same U term on Ti atoms will give the same description of those defects where electrons are trapped on Ti sites, such as \square_{O} . For \square_{Ti} where PBE+ U [Ti,O] yields larger electrons localized on the oxygen $2p$ orbitals, the agreement between PBE+ U [Ti] and PBE+ U [Ti,O] is worse. One point that is noticeable in Table III is that the agreement between HSE15 and PBEsol, once the VBM have been aligned, is rather good (MAE of 0.26 eV) so that standard semilocal functionals might be a better choice for a first estimation of the defect energetics, assuming the valence band maxima have been aligned with those of a more accurate functional. This ability of semilocal functionals to give thermodynamic charge transition levels and defect formation energies in a rather good agreement with hybrid functionals is consistent with studies of other semiconductor materials, see for example references 23 and 27. It is somewhat surprising that the agreement between the PBE+ U approaches and HSE15 is the worst. One should have expected a better agreement as both PBE+ U and hybrid functionals partly correct for the self-interaction error which largely affects electron localization and thus the properties of the point defect. A more detailed analysis for the understanding of the factors that affect the values of charge transitions levels and defect formation energies calculated with different functionals is in order.

Taking the \square_{O} , the main difference between PBEsol comes from the non-charged state being relatively more stable using HSE15, which results in a direct transition level from the +2 state to the noncharged state close to the CBM. Figure 3 shows a comparison of the geometric structure and defect-induced charge density of the neutral \square_{O} as obtained by the various xc functionals

considered in this study. Removing an oxygen atom from pristine anatase reduces the point group symmetry to $mm2$. However, a more stable lower symmetry ($\bar{2}$ point group) configuration, named a “split-vacancy” in an earlier GGA+ U study[54], can be found, Figure 3. We were able to find these two configurations for all the employed functionals and found that the low-symmetry configuration has the lower energy than the high-symmetry one, even though the difference is sometimes small: 0.14 eV for PBEsol, 0.77 eV for PBE+ U [Ti] and 0.38 eV for HSE15. As one can see from Figure 3, the symmetry breaking that characterizes the split-vacancy configuration is driven by electron localization on neighboring Ti atoms. Due to the self-interaction and band-gap errors, in PBEsol \square_O induces a defective level which is mixed with the bottom of the conduction band and the extra electrons are therefore delocalized on several Ti atoms. For this reason, the local distortions leading to the $\bar{2}$ symmetry are minimal. If we consider the PBE+ U approach instead, the electron localization is much stronger and affects mainly two distinct Ti atoms which become reduced to the +3 state. As a consequence, the local geometric distortions are also much more relevant, such features are found both with PBE+ U [Ti] and PBE+ U [Ti,O]. Also HSE15 predicts the defect state to be localized, albeit to a lesser degree than PBE+ U . Taking HSE15 results as a reference, it is then evident that semilocal functionals tend to disfavor the localized solution due to self-interaction error. On the other hand, PBE+ U tends to overlocalize the electrons. For this approach, the ability to describe electron localization is governed by the U term, and a value which gives a reliable description of the property of the host material (such as band gap and cell parameters) is not necessarily suitable for describing the defective system. We mention that previous HSE studies[15, 16] only considered the high-symmetry configuration which would lead to an overestimation of the energy of the non-charged \square_O defect.

These results underline an important advantage of the PBE+ U approach: even if the total energies have limited predictive value when comparing different oxidation states, PBE+ U allows a computationally relatively efficient exploration of the potential energy surface where also structures characterized by localized states are present. These can then serve as a starting points for more time consuming methodologies like the use of hybrid functionals.

Analogous considerations hold for the other studied defects. In particular, we show in Figure 4 the comparison for the most relevant electron acceptor: the \square_{Ti} . We choose the completely ionized (4-) defect state in order to emphasize the behaviour of localized electrons. In this charge state, four electrons have been accepted from the host material and the defect-induced levels are filled. From Figure 4 one can see that the PBE+ U approach predicts electron localization mostly on four

oxygen atoms neighboring the vacancy: two oxygen atoms are the nearest neighbors located on the line parallel to the [001] direction and other two oxygen atoms are the closest neighbors along the line parallel to the [010] direction. Electron localization on these sites is similarly predicted by the PBE+ U [Ti] and PBE+ U [Ti, O] schemes, but in the latter more electrons are localized on the former two oxygen atoms than the latter two. Once more, the extra charge is more delocalized in PBEsol. The HSE15 predicts a rather localized electronic configuration, especially on the two oxygen atoms along the [001] direction, but to a noticeably lesser degree than in PBE+ U .

D. Bulk Thermochemistry

Calculated values for the formation enthalpies of selected titanium oxides are reported in Table IV. We took those compounds whose crystal structures and experimental formation enthalpies are well described on the NIST-JANAF thermochemical tables [55]. In particular, we took: TiO₂ anatase, TiO₂ rutile, Ti₂O₃, Ti₃O₅ and TiO. TiO₂ rutile has a tetragonal primitive cell (space group $P4_2/mnm$) and it is a semiconductor with a band gap of 3.0 eV [56]. For Ti₂O₃, we took the rhombohedral phase (space group $R\bar{3}c$) which is commonly found at room temperature. Its ground state is non-magnetic and the system is a semiconductor with a very small band gap of around 0.1 eV, given by a trigonal crystal field distortion that splits the occupied Ti $3d a_{1g}$ states from the unoccupied $3d e_g$ ones [57]. The computational modeling of this phase is challenging. PBEsol predicts a metal while with PBE+ U [Ti] we obtain a very large band gap of around 1 eV. Moreover, PBE+ U [Ti] finds that the antiferromagnetic state has a much lower energy than the diamagnetic one. Due to these problems, we excluded such compound from the fitting procedure described by Jain *et al.* [58]. Ti₃O₅ was taken in the low-symmetry phase which is stable for temperatures below 120°C and has the monoclinic structure (space group $C2/m$)[59]. It is a semiconductor with a small gap of 0.14 eV, which also arises from the splitting of the Ti $3d$ states [60]. While semi-local functionals predict it to be a metal, the DFT+ U approach correctly describes the semiconductor state [61]. Finally, TiO has the NaCl structure, with a cubic cell and space group $Fm\bar{3}m$. This compound is metallic [62] and was therefore not calculated using the PBE+ U setup.

As shown by Table IV, both PBEsol and PBE+ U predict the ground state of the TiO₂ system to be anatase. We found that anatase is also more stable than rutile using HSE15, which predicts anatase to be more stable than rutile by around 93 meV per formula unit. Regarding the other phases, PBEsol gives formation enthalpies in good agreement with the experimental data. That

this is the case, despite the varying oxidation states, is somewhat surprising, as the self-interaction error should favor states with a smaller number of localized d electrons, *i.e.* more oxidized states. However, GGA functionals tend also to overbind the O_2 molecule [63]. This overbinding will on the other hand favor more reduced states, and the good agreement observed for PBEsol can to a certain degree be attributed to this cancellation of errors.

In the employed DFT+ U formulation[22, 36], an energy contribution of the form:

$$\sum_{\sigma} \frac{U}{2} \text{Tr}[\mathbf{n}_{\sigma}(1 - \mathbf{n}_{\sigma})] \quad (4)$$

is added to the energy functional. U quantifies an effective on-site coulombic repulsion that is applied to chosen atomic sites. σ is the spin variable and \mathbf{n} the occupation number matrix in the localized orbital representation. The energy contribution is positive for all fractional occupation numbers and it so increases the energy of Ti-O systems, where the d -orbitals are not fully localized. This results in a large positive energy contribution to all systems where the U is applied. In the present case, where we would not apply the U for the Ti metal, this would lead to a strong underestimation of the energy gain by forming the oxide, as shown in the column “PBE+ U [Ti]” of Table IV, which reports the calculated formation enthalpies where the Hubbard U is used for the non-metallic oxides of titanium. It is then clear that formation enthalpies obtaining by mixing PBE and PBE+ U calculations do not have any physical meaning. To improve on this, Jain *et al.* proposed a method that adjusts the energies calculated with GGA+ U in such a way that they can be mixed with pure GGA calculations [58]. Their method is based on fitting formation energies of binary transition metal oxides in order to find a correction term per transition metal atom that has to be added to the calculated GGA+ U energies [58]. The value of the correction term we found from this fitting is of $\Delta E_{\text{Ti}} = 2.89$ eV per Ti atom. The results obtained after adding this correction together with the correction term for the GGA overbinding[63] are summarized in the "Corrected" column “PBE+ U [Ti] Corrected”. Of course, applying such correction will drastically improve the calculated formation enthalpies for the compounds included in the fitting: the MAE drops to 14 meV/atom.

An accurate determination of the thermochemistry of the relevant phases is important in the calculation of defect formation energies as it determines the limit values of the chemical potentials of Ti and O. From the experimental formation enthalpies it results that the first phase that starts to precipitate in Ti-rich conditions is Ti_2O_3 . In order to obtain the competing phases in such a limiting conditions as predicted by the various xc functionals we calculated the convex hull of

the Ti-O systems. Figure 5 shows the hull calculated using the PBE+ U [Ti] setup with Jain *et al.*'s correction scheme (PBE+ U [Ti] Corrected). In order to calculate the hull, we started from the compounds and energies available on the AFLOW repositories [64, 65], we performed a first screening and selected all the compounds lying within 0.25 eV/atom from the convex hull. For such compounds, we then calculated the total energies using our PBE+ U [Ti] scheme and recalculated the convex hull using the new energies corrected with Jain *et al.*'s method. From these calculations, we found that the first phase that precipitates in Ti-rich conditions is not the non-magnetic phase of Ti_2O_3 but the anti-ferromagnetic one, which lies on the convex hull in Figure 5. The non-magnetic phase of Ti_2O_3 has a much larger energy and considering it as the ground state phase would make Ti_3O_5 to be the first compound to segregate in Ti-rich conditions. This shows that care must be taken when one attempts to calculate the value of the chemical potentials of Ti and O in the Ti-rich and O-rich limits from functionals which do not correctly describe the thermochemistry of the system.

Table V reports the values of the chemical potentials, with respect to their standard state, calculated using different methods for the O-rich and Ti-rich limits and considering only phase competition between anatase, the sesquioxide (in the ground state electronic structure predicted by that functional) and pure Ti and O_2 . We can notice that the ranges of μ_{O} and μ_{Ti} for O-rich conditions agree well among PBEsol, PBE+ U [Ti], HSE06 (obtained from reference [15]) and the experimental data. For PBE+ U [Ti] this happens since both the energy of the O_2 molecule and of anatase are fitted to experimental data, as described above. While, as we mentioned before, PBEsol is expected to be affected both by the GGA shortcomings in the binding energy of O_2 and by the self-interaction error, which tend to compensate in pure GGA functionals and a good agreement with the experiment is found.

If Ti-rich conditions are considered, now the relevant phases for determining the chemical potential ranges, as found from experimental data, are TiO_2 anatase and Ti_2O_3 . While HSE06 does a fairly good job in predicting the thermochemistry of transition-metal compounds, as already mentioned, compensation of errors are present in PBEsol, which also gives values close to the experimental ones. Also the corrected PBE+ U [Ti] results tend to agree with the experimental ones; but while both PBEsol and HSE15 predict a value of $\Delta\mu_{\text{Ti}}$ larger than the one derived from experimental data, the corrected PBE+ U [Ti] predicts smaller values. Such discrepancy would add another source of disagreement between functionals on the calculated defect formation energies in the Ti-rich limit.

E. Defect Formation Energies

We calculated defect formation energies in the O-rich limit, where the chemical potential of the oxygen is set equal to half the electronic energy predicted for O_2 and the relevant thermochemistry is in good agreement among all xc functionals and experiments as well, and compare them among the different employed xc functionals, as shown in Figure ???. The analysis performed in Section III D should make obvious that formation energies obtained by mixing GGA+ U and GGA are unreliable without applying some correction scheme. We thus compared only the formation energies calculated with PBEsol, the corrected PBE+ U [Ti] and HSE15 after the band alignment procedure.

One can notice that the agreement between calculated formation energies is quite poor and that the MAEs are quite large: 0.92 eV between PBE+ U [Ti] and PBEsol, 1.2 eV between the corrected PBE+ U [Ti] and HSE15. the best agreement is obtained between PBEsol and HSE15, with a MAE of 0.41 eV which is comparable to the one found between PBE and HSE06 for GaN defects [26]. One also notices that while PBEsol gives almost exclusively defect formation energies which are smaller than those predicted by HSE15, the formation energies predicted by the corrected PBE+ U [Ti] do not follow a general trend. This also partly explains why the transition levels predicted with this functional are in such a poor agreement with HSE15, as transition levels are given by differences in defect formation energies.

To end this section, we assess the effect of fixing cell parameters to experimental values or values that do not correspond to the ground state predicted by given functional for anatase. For this purpose we used the corrected PBE+ U [Ti] scheme in order to calculate the formation energies of point defects in two cases: in the first case, the cell parameter was fixed to the value predicted by the PBE+ U [Ti] method. We call this choice of cell “cell 1”. In the second case, we instead fixed the cell parameter to the value predicted by PBEsol, which is in better agreement with the experimental one. We refer to this second choice of cell parameter as “cell 2”. PBE+ U [Ti] overestimates the cell parameter of anatase; this entails that using “cell 2” induces a large external pressure on the supercell, from the diagonal part of the stress tensor we found that such pressure is very large, around 16 GPa. Figure ?? summarizes the differences in formation energies predicted using the two different cells. As expected, using “cell 2” overestimates the defect formation energy, since an external pressure is applied on the supercell. While the MAE is quite large, around 0.77 eV, we notice that for the largest part, the discrepancy can be assigned to the Ti_i and Ti_O classes of

defects. This is not surprising as we mentioned before that both defects exert a large strain on the host material since they are characterized by the presence of an atom such as Ti, with a large atomic radius, occupying an interstitial site. Therefore, fixing cell parameters to values other than those predicted by the used theoretical scheme, can lead to considerable errors if the considered defects induce large strains on the crystal and is not a recommendable practice.

IV. CONCLUSIONS

In summary, we have found several factors that can affect the values of defect formation energies and charge transition levels in anatase and make comparisons between different functionals difficult.

Considering charge transition levels and defect formation energies, we find that, after band edges have been properly aligned to a common reference, the best agreement between functionals are found to occur between the PBEsol approaches and HSE15. This fact appears counter intuitive as PBE+ U is able to give defect geometric and electronic structures in closer agreement to HSE15 than PBEsol, by partly correcting for self-interaction errors. Also when defect formation energies are considered, there is a fair agreement between PBEsol and HSE15 values.

These observations suggest that although semilocal functionals are inadequate to correctly describe the geometric and electronic properties of defect where charge-localization is relevant, they might be a good choice for a first estimation of the energetic properties of point defects in semiconductors, assuming the valence band maximum is correctly aligned using a more accurate functional. On the other hand, the use of DFT+ U is advantageous for obtaining a more accurate initial geometric and electronic configuration which can be used as a starting point for more accurate and computationally expensive functionals.

V. ACKNOWLEDGMENTS

The authors acknowledge support from the Austrian Science Funds (FWF) under project CODIS (FWF-I-3576-N36). We also thank the Vienna Scientific Cluster for providing the com-

putational facilities (1523306: CODIS).

- [1] Amy L. Linsebigler, Guangquan Lu, and John T. Yates. Photocatalysis on tio2 surfaces: Principles, mechanisms, and selected results. *Chemical Reviews*, 95(3):735–758, May 1995. ISSN 0009-2665. doi:10.1021/cr00035a013. URL <https://doi.org/10.1021/cr00035a013>.
- [2] Jenny Schneider, Masaya Matsuoka, Masato Takeuchi, Jinlong Zhang, Yu Horiuchi, Masakazu Anpo, and Detlef W. Bahnemann. Understanding tio2 photocatalysis: Mechanisms and materials. *Chemical Reviews*, 114(19):9919–9986, Oct 2014. ISSN 0009-2665. doi:10.1021/cr5001892. URL <https://doi.org/10.1021/cr5001892>.
- [3] Taishi Sumita, Tetsuya Yamaki, Shunya Yamamoto, and Atsumi Miyashita. Photo-induced surface charge separation of highly oriented tio2 anatase and rutile thin films. *Applied Surface Science*, 200(1): 21 – 26, 2002. ISSN 0169-4332. doi:[https://doi.org/10.1016/S0169-4332\(02\)00614-1](https://doi.org/10.1016/S0169-4332(02)00614-1). URL <http://www.sciencedirect.com/science/article/pii/S0169433202006141>.
- [4] Tim Luttrell, Sandamali Halpegamage, Junguang Tao, Alan Kramer, Eli Sutter, and Matthias Batzill. Why is anatase a better photocatalyst than rutile?: - model studies on epitaxial tio2 films. *Scientific Reports*, 4:4043 EP –, Feb 2014. URL <https://doi.org/10.1038/srep04043>. Article.
- [5] L. Kavan, M. Grätzel, S. E. Gilbert, C. Klemenz, and H. J. Scheel. Electrochemical and photoelectrochemical investigation of single-crystal anatase. *Journal of the American Chemical Society*, 118(28):6716–6723, Jan 1996. ISSN 0002-7863. doi:10.1021/ja954172l. URL <https://doi.org/10.1021/ja954172l>.
- [6] L. Forro, O. Chauvet, D. Emin, L. Zuppiroli, H. Berger, and F. Lévy. High mobility n-type charge carriers in large single crystals of anatase (tio2). *Journal of Applied Physics*, 75(1):633–635, 1994. doi:10.1063/1.355801. URL <https://doi.org/10.1063/1.355801>.
- [7] Yutaka Furubayashi, Taro Hitosugi, Yukio Yamamoto, Kazuhisa Inaba, Go Kinoda, Yasushi Hirose, Toshihiro Shimada, and Tetsuya Hasegawa. A transparent metal: Nb-doped anatase tio2. *Applied Physics Letters*, 86(25):252101, 2005. doi:10.1063/1.1949728. URL <https://doi.org/10.1063/1.1949728>.
- [8] T. Hitosugi, Y. Furubayashi, A. Ueda, K. Itabashi, K. Inaba, Y. Hirose, G. Kinoda, Y. Yamamoto, T. Shimada, and T. Hasegawa. Ta-doped Anatase TiO₂ Epitaxial Film as Transparent Conducting Oxide. *Japanese Journal of Applied Physics*, 44:L1063–L1065, August 2005. doi:

10.1143/JJAP.44.L1063.

- [9] Ulrike Diebold. The surface science of titanium dioxide. *Surface Science Reports*, 48(5):53 – 229, 2003. ISSN 0167-5729. doi:[https://doi.org/10.1016/S0167-5729\(02\)00100-0](https://doi.org/10.1016/S0167-5729(02)00100-0). URL <http://www.sciencedirect.com/science/article/pii/S0167572902001000>.
- [10] Stefan Wendt, Phillip T. Sprunger, Estephania Lira, Georg K. H. Madsen, Zheshen Li, Jonas Ø. Hansen, Jesper Matthiesen, Asger Blekinge-Rasmussen, Erik Lægsgaard, Bjørk Hammer, and Flemming Besenbacher. The role of interstitial sites in the Ti^{3d} defect state in the band gap of titania. *Science*, 320(5884):1755–1759, 2008. ISSN 0036-8075. doi:10.1126/science.1159846. URL <https://science.sciencemag.org/content/320/5884/1755>.
- [11] Wen-Jin Yin, Bo Wen, Chuanyao Zhou, Annabella Selloni, and Li-Min Liu. Excess electrons in reduced rutile and anatase TiO_2 . *Surface Science Reports*, 73(2):58 – 82, 2018. ISSN 0167-5729. doi:<https://doi.org/10.1016/j.surfrep.2018.02.003>. URL <http://www.sciencedirect.com/science/article/pii/S0167572918300128>.
- [12] Sutassana Na-Phattalung, M. F. Smith, Kwiseon Kim, Mao-Hua Du, Su-Huai Wei, S. B. Zhang, and Sukit Limpijumnong. First-principles study of native defects in anatase TiO_2 . *Phys. Rev. B*, 73:125205, Mar 2006. doi:10.1103/PhysRevB.73.125205. URL <https://link.aps.org/doi/10.1103/PhysRevB.73.125205>.
- [13] Jorge Osorio-Guillén, Stephan Lany, and Alex Zunger. Atomic control of conductivity versus ferromagnetism in wide-gap oxides via selective doping: V, Nb, Ta in anatase TiO_2 . *Phys. Rev. Lett.*, 100:036601, Jan 2008. doi:10.1103/PhysRevLett.100.036601. URL <https://link.aps.org/doi/10.1103/PhysRevLett.100.036601>.
- [14] Benjamin J. Morgan and Graeme W. Watson. Polaronic trapping of electrons and holes by native defects in anatase TiO_2 . *Phys. Rev. B*, 80:233102, Dec 2009. doi:10.1103/PhysRevB.80.233102. URL <https://link.aps.org/doi/10.1103/PhysRevB.80.233102>.
- [15] Adisak Boonchun, Pakpoom Reunchan, and Naoto Umezawa. Energetics of native defects in anatase TiO_2 : a hybrid density functional study. *Phys. Chem. Chem. Phys.*, 18:30040–30046, 2016. doi:10.1039/C6CP05798E. URL <http://dx.doi.org/10.1039/C6CP05798E>.
- [16] Peter Deák, Bálint Aradi, and Thomas Frauenheim. Oxygen deficiency in TiO_2 : Similarities and differences between the Ti self-interstitial and the O vacancy in bulk rutile and anatase. *Phys. Rev. B*, 92:045204, Jul 2015. doi:10.1103/PhysRevB.92.045204. URL <https://link.aps.org/doi/10.1103/PhysRevB.92.045204>.

- [17] Jochen Heyd, Gustavo E. Scuseria, and Matthias Ernzerhof. Hybrid functionals based on a screened coulomb potential. *The Journal of Chemical Physics*, 118(18):8207–8215, 2003. doi: 10.1063/1.1564060. URL <https://doi.org/10.1063/1.1564060>.
- [18] Stephan Lany and Alex Zunger. Assessment of correction methods for the band-gap problem and for finite-size effects in supercell defect calculations: Case studies for zno and gaas. *Phys. Rev. B*, 78:235104, Dec 2008. doi:10.1103/PhysRevB.78.235104. URL <https://link.aps.org/doi/10.1103/PhysRevB.78.235104>.
- [19] Peter Deák, Adam Gali, Bálint Aradi, and Thomas Frauenheim. Accurate gap levels and their role in the reliability of other calculated defect properties. *physica status solidi (b)*, 248(4):790–798, 2011. doi:10.1002/pssb.201046210. URL <https://onlinelibrary.wiley.com/doi/abs/10.1002/pssb.201046210>.
- [20] John P. Perdew, Robert G. Parr, Mel Levy, and Jose L. Balduz. Density-functional theory for fractional particle number: Derivative discontinuities of the energy. *Phys. Rev. Lett.*, 49:1691–1694, Dec 1982. doi:10.1103/PhysRevLett.49.1691. URL <https://link.aps.org/doi/10.1103/PhysRevLett.49.1691>.
- [21] Benjamin G. Janesko, Thomas M. Henderson, and Gustavo E. Scuseria. Screened hybrid density functionals for solid-state chemistry and physics. *Phys. Chem. Chem. Phys.*, 11:443–454, 2009. doi: 10.1039/B812838C. URL <http://dx.doi.org/10.1039/B812838C>.
- [22] V. I. Anisimov, I. V. Solovyev, M. A. Korotin, M. T. Czyżyk, and G. A. Sawatzky. Density-functional theory and nio photoemission spectra. *Phys. Rev. B*, 48:16929–16934, Dec 1993. doi: 10.1103/PhysRevB.48.16929. URL <https://link.aps.org/doi/10.1103/PhysRevB.48.16929>.
- [23] Audrius Alkauskas, Peter Broqvist, and Alfredo Pasquarello. Defect energy levels in density functional calculations: Alignment and band gap problem. *Phys. Rev. Lett.*, 101:046405, Jul 2008. doi: 10.1103/PhysRevLett.101.046405. URL <https://link.aps.org/doi/10.1103/PhysRevLett.101.046405>.
- [24] Audrius Alkauskas and Alfredo Pasquarello. Band-edge problem in the theoretical determination of defect energy levels: The o vacancy in zno as a benchmark case. *Phys. Rev. B*, 84:125206, Sep 2011. doi:10.1103/PhysRevB.84.125206. URL <https://link.aps.org/doi/10.1103/PhysRevB.84.125206>.
- [25] R. Ramprasad, H. Zhu, Patrick Rinke, and Matthias Scheffler. New perspective on formation energies and energy levels of point defects in nonmetals. *Phys. Rev. Lett.*, 108:066404, Feb 2012. doi:

- 10.1103/PhysRevLett.108.066404. URL <https://link.aps.org/doi/10.1103/PhysRevLett.108.066404>.
- [26] Christoph Freysoldt, Björn Lange, Jörg Neugebauer, Qimin Yan, John L. Lyons, Anderson Janotti, and Chris G. Van de Walle. Electron and chemical reservoir corrections for point-defect formation energies. *Phys. Rev. B*, 93:165206, Apr 2016. doi:10.1103/PhysRevB.93.165206. URL <https://link.aps.org/doi/10.1103/PhysRevB.93.165206>.
- [27] John L. Lyons and Chris G. Van de Walle. Computationally predicted energies and properties of defects in gan. *npj Computational Materials*, 3(1):12, 2017. ISSN 2057-3960. doi:10.1038/s41524-017-0014-2. URL <https://doi.org/10.1038/s41524-017-0014-2>.
- [28] S. B. Zhang and John E. Northrup. Chemical potential dependence of defect formation energies in gaas: Application to ga self-diffusion. *Phys. Rev. Lett.*, 67:2339–2342, Oct 1991. doi:10.1103/PhysRevLett.67.2339. URL <https://link.aps.org/doi/10.1103/PhysRevLett.67.2339>.
- [29] Tor S. Bjørheim, Marco Arrigoni, Denis Gryaznov, Eugene Kotomin, and Joachim Maier. Thermodynamic properties of neutral and charged oxygen vacancies in bazro3 based on first principles phonon calculations. *Phys. Chem. Chem. Phys.*, 17:20765–20774, 2015. doi:10.1039/C5CP02529J. URL <http://dx.doi.org/10.1039/C5CP02529J>.
- [30] Tor S. Bjørheim, Marco Arrigoni, Sarmad W. Saeed, Eugene Kotomin, and Joachim Maier. Surface segregation entropy of protons and oxygen vacancies in bazro3. *Chemistry of Materials*, 28(5):1363–1368, Mar 2016. ISSN 0897-4756. doi:10.1021/acs.chemmater.5b04327. URL <https://doi.org/10.1021/acs.chemmater.5b04327>.
- [31] Marco Arrigoni, Tor S. Bjørheim, Eugene Kotomin, and Joachim Maier. First principles study of confinement effects for oxygen vacancies in bazro3 (001) ultra-thin films. *Phys. Chem. Chem. Phys.*, 18:9902–9908, 2016. doi:10.1039/C6CP00830E. URL <http://dx.doi.org/10.1039/C6CP00830E>.
- [32] A. Glensk, B. Grabowski, T. Hickel, and J. Neugebauer. Breakdown of the arrhenius law in describing vacancy formation energies: The importance of local anharmonicity revealed by ab initio thermodynamics. *Phys. Rev. X*, 4:011018, Feb 2014. doi:10.1103/PhysRevX.4.011018. URL <https://link.aps.org/doi/10.1103/PhysRevX.4.011018>.
- [33] Christoph Freysoldt, Blazej Grabowski, Tilmann Hickel, Jörg Neugebauer, Georg Kresse, Anderson Janotti, and Chris G. Van de Walle. First-principles calculations for point defects in solids. *Rev. Mod. Phys.*, 86:253–305, Mar 2014. doi:10.1103/RevModPhys.86.253. URL <https://link.aps.org/>

doi/10.1103/RevModPhys.86.253.

- [34] Yu Kumagai and Fumiyasu Oba. Electrostatics-based finite-size corrections for first-principles point defect calculations. *Phys. Rev. B*, 89:195205, May 2014. doi:10.1103/PhysRevB.89.195205. URL <https://link.aps.org/doi/10.1103/PhysRevB.89.195205>.
- [35] John P. Perdew, Adrienn Ruzsinszky, Gábor I. Csonka, Oleg A. Vydrov, Gustavo E. Scuseria, Lucian A. Constantin, Xiaolan Zhou, and Kieron Burke. Restoring the density-gradient expansion for exchange in solids and surfaces. *Phys. Rev. Lett.*, 100:136406, Apr 2008. doi:10.1103/PhysRevLett.100.136406. URL <https://link.aps.org/doi/10.1103/PhysRevLett.100.136406>.
- [36] S. L. Dudarev, G. A. Botton, S. Y. Savrasov, C. J. Humphreys, and A. P. Sutton. Electron-energy-loss spectra and the structural stability of nickel oxide: An lsda+u study. *Phys. Rev. B*, 57:1505–1509, Jan 1998. doi:10.1103/PhysRevB.57.1505. URL <https://link.aps.org/doi/10.1103/PhysRevB.57.1505>.
- [37] Vladimir I. Anisimov, Jan Zaanen, and Ole K. Andersen. Band theory and mott insulators: Hubbard u instead of stoner i. *Phys. Rev. B*, 44:943–954, Jul 1991. doi:10.1103/PhysRevB.44.943. URL <https://link.aps.org/doi/10.1103/PhysRevB.44.943>.
- [38] P. E. Blöchl. Projector augmented-wave method. *Phys. Rev. B*, 50:17953–17979, Dec 1994. doi:10.1103/PhysRevB.50.17953. URL <https://link.aps.org/doi/10.1103/PhysRevB.50.17953>.
- [39] G. Kresse and J. Furthmüller. Efficient iterative schemes for ab initio total-energy calculations using a plane-wave basis set. *Phys. Rev. B*, 54:11169–11186, Oct 1996. doi:10.1103/PhysRevB.54.11169. URL <https://link.aps.org/doi/10.1103/PhysRevB.54.11169>.
- [40] Stefano Baroni and Raffaele Resta. Ab initio calculation of the macroscopic dielectric constant in silicon. *Phys. Rev. B*, 33:7017–7021, May 1986. doi:10.1103/PhysRevB.33.7017. URL <https://link.aps.org/doi/10.1103/PhysRevB.33.7017>.
- [41] M. Gajdoš, K. Hummer, G. Kresse, J. Furthmüller, and F. Bechstedt. Linear optical properties in the projector-augmented wave methodology. *Phys. Rev. B*, 73:045112, Jan 2006. doi:10.1103/PhysRevB.73.045112. URL <https://link.aps.org/doi/10.1103/PhysRevB.73.045112>.
- [42] Vladan Stevanović, Stephan Lany, David S. Ginley, Willam Tumas, and Alex Zunger. Assessing capability of semiconductors to split water using ionization potentials and electron affinities only. *Phys. Chem. Chem. Phys.*, 16:3706–3714, 2014. doi:10.1039/C3CP54589J. URL <http://dx.doi.org/10.1039/C3CP54589J>.

org/10.1039/C3CP54589J.

- [43] J. L. Lyons, A. Janotti, and C. G. Van de Walle. Role of si and ge as impurities in zno. *Phys. Rev. B*, 80:205113, Nov 2009. doi:10.1103/PhysRevB.80.205113. URL <https://link.aps.org/doi/10.1103/PhysRevB.80.205113>.
- [44] Yoyo Hinuma, Andreas Grüneis, Georg Kresse, and Fumiyasu Oba. Band alignment of semiconductors from density-functional theory and many-body perturbation theory. *Phys. Rev. B*, 90:155405, Oct 2014. doi:10.1103/PhysRevB.90.155405. URL <https://link.aps.org/doi/10.1103/PhysRevB.90.155405>.
- [45] K. V. Krishna Rao, S. V. Nagender Naidu, and Leela Iyengar. Thermal expansion of rutile and anatase. *Journal of the American Ceramic Society*, 53(3):124–126, 1970. doi:10.1111/j.1151-2916.1970.tb12051.x. URL <https://ceramics.onlinelibrary.wiley.com/doi/abs/10.1111/j.1151-2916.1970.tb12051.x>.
- [46] R. J. Gonzalez, R. Zallen, and H. Berger. Infrared reflectivity and lattice fundamentals in anatase TiO_2 s. *Phys. Rev. B*, 55:7014–7017, Mar 1997. doi:10.1103/PhysRevB.55.7014. URL <https://link.aps.org/doi/10.1103/PhysRevB.55.7014>.
- [47] Burak Himmetoglu, Andrea Floris, Stefano de Gironcoli, and Matteo Cococcioni. Hubbard-corrected dft energy functionals: The lda+u description of correlated systems. *International Journal of Quantum Chemistry*, 114(1):14–49, 2014. doi:10.1002/qua.24521. URL <https://onlinelibrary.wiley.com/doi/abs/10.1002/qua.24521>.
- [48] Emanuele Finazzi, Cristiana Di Valentin, and Gianfranco Pacchioni. Nature of ti interstitials in reduced bulk anatase and rutile TiO_2 . *The Journal of Physical Chemistry C*, 113(9):3382–3385, Mar 2009. ISSN 1932-7447. doi:10.1021/jp8111793. URL <https://doi.org/10.1021/jp8111793>.
- [49] Hideyuki Kamisaka and Koichi Yamashita. Theoretical study of the interstitial oxygen atom in anatase and rutile TiO_2 : Electron trapping and elongation of the r(o-o) bond. *The Journal of Physical Chemistry C*, 115(16):8265–8273, Apr 2011. ISSN 1932-7447. doi:10.1021/jp110648q. URL <https://doi.org/10.1021/jp110648q>.
- [50] Emanuele Finazzi, Cristiana Di Valentin, Gianfranco Pacchioni, and Annabella Selloni. Excess electron states in reduced bulk anatase TiO_2 : Comparison of standard gga, gga+u, and hybrid dft calculations. *The Journal of Chemical Physics*, 129(15):154113, 2008. doi:10.1063/1.2996362. URL <https://doi.org/10.1063/1.2996362>.

- [51] Koichi Momma and Fujio Izumi. *VESTA3* for three-dimensional visualization of crystal, volumetric and morphology data. *Journal of Applied Crystallography*, 44(6):1272–1276, Dec 2011. doi:10.1107/S0021889811038970. URL <https://doi.org/10.1107/S0021889811038970>.
- [52] Clelia Spreafico and Joost VandeVondele. The nature of excess electrons in anatase and rutile from hybrid dft and rpa. *Phys. Chem. Chem. Phys.*, 16:26144–26152, 2014. doi:10.1039/C4CP03981E. URL <http://dx.doi.org/10.1039/C4CP03981E>.
- [53] Martin Setvin, Cesare Franchini, Xianfeng Hao, Michael Schmid, Anderson Janotti, Merzuk Kaltak, Chris G. Van de Walle, Georg Kresse, and Ulrike Diebold. Direct view at excess electrons in TiO_2 rutile and anatase. *Phys. Rev. Lett.*, 113:086402, Aug 2014. doi:10.1103/PhysRevLett.113.086402. URL <https://link.aps.org/doi/10.1103/PhysRevLett.113.086402>.
- [54] Benjamin J. Morgan and Graeme W. Watson. Intrinsic n-type defect formation in TiO_2 : A comparison of rutile and anatase from gga+u calculations. *The Journal of Physical Chemistry C*, 114(5):2321–2328, Feb 2010. ISSN 1932-7447. doi:10.1021/jp9088047. URL <https://doi.org/10.1021/jp9088047>.
- [55] Jr Malcolm W. Chase. *NIST-JANAF thermochemical tables*. Fourth edition. Washington, DC : American Chemical Society ; New York : American Institute of Physics for the National Institute of Standards and Technology, 1998., 1998. URL <https://search.library.wisc.edu/catalog/999842910902121>. Issued as: Journal of physical and chemical reference data; monograph no. 9, 1998.;Includes bibliographies.
- [56] D Reyes-Coronado, G Rodríguez-Gattorno, M E Espinosa-Pesqueira, C Cab, R de Coss, and G Oskam. Phase-pure TiO_2 nanoparticles: anatase, brookite and rutile. *Nanotechnology*, 19(14):145605, mar 2008. doi:10.1088/0957-4484/19/14/145605. URL <https://doi.org/10.1088/0957-4484/19/14/145605>.
- [57] Yuzheng Guo, Stewart J Clark, and John Robertson. Electronic and magnetic properties of TiO_3 , CrO_3 , and FeO_3 calculated by the screened exchange hybrid density functional. *Journal of Physics: Condensed Matter*, 24(32):325504, jul 2012. doi:10.1088/0953-8984/24/32/325504. URL <https://doi.org/10.1088/0953-8984/24/32/325504>.
- [58] Anubhav Jain, Geoffroy Hautier, Shyue Ping Ong, Charles J. Moore, Christopher C. Fischer, Kristin A. Persson, and Gerbrand Ceder. Formation enthalpies by mixing gga and gga + u calculations. *Phys. Rev. B*, 84:045115, Jul 2011. doi:10.1103/PhysRevB.84.045115. URL <https://link.aps.org/doi/10.1103/PhysRevB.84.045115>.

- [59] S. Åsbrink and A. Magnéli. Crystal structure studies on trititanium pentoxide, Ti_3O_5 . *Acta Crystallographica*, 12(8):575–581, Aug 1959. doi:10.1107/S0365110X59001694. URL <https://doi.org/10.1107/S0365110X59001694>.
- [60] Shin-ichi Ohkoshi, Yoshihide Tsunobuchi, Tomoyuki Matsuda, Kazuhito Hashimoto, Asuka Namai, Fumiyoshi Hakoe, and Hiroko Tokoro. Synthesis of a metal oxide with a room-temperature photoreversible phase transition. *Nature Chemistry*, 2:539 EP –, May 2010. URL <https://doi.org/10.1038/nchem.670>. Article.
- [61] Rui Liu, Jia-Xiang Shang, and Fu-He Wang. Electronic, magnetic and optical properties of β - Ti_3O_5 and λ - Ti_3O_5 : A density functional study. *Computational Materials Science*, 81:158 – 162, 2014. ISSN 0927-0256. doi:<https://doi.org/10.1016/j.commatsci.2013.08.001>. URL <http://www.sciencedirect.com/science/article/pii/S0927025613004527>.
- [62] Stephen Paul Denker. Electronic properties of titanium monoxide. *Journal of Applied Physics*, 37(1): 142–149, 1966. doi:10.1063/1.1707796. URL <https://doi.org/10.1063/1.1707796>.
- [63] Lei Wang, Thomas Maxisch, and Gerbrand Ceder. Oxidation energies of transition metal oxides within the GGA + U framework. *Phys. Rev. B*, 73:195107, May 2006. doi:10.1103/PhysRevB.73.195107. URL <https://link.aps.org/doi/10.1103/PhysRevB.73.195107>.
- [64] Stefano Curtarolo, Wahyu Setyawan, Shidong Wang, Junkai Xue, Kesong Yang, Richard H. Taylor, Lance J. Nelson, Gus L.W. Hart, Stefano Sanvito, Marco Buongiorno-Nardelli, Natalio Mingo, and Ohad Levy. Aflowlib.org: A distributed materials properties repository from high-throughput ab initio calculations. *Computational Materials Science*, 58:227 – 235, 2012. ISSN 0927-0256. doi:<https://doi.org/10.1016/j.commatsci.2012.02.002>. URL <http://www.sciencedirect.com/science/article/pii/S0927025612000687>.
- [65] Richard H. Taylor, Frisco Rose, Cormac Toher, Ohad Levy, Kesong Yang, Marco Buongiorno Nardelli, and Stefano Curtarolo. A restful api for exchanging materials data in the aflowlib.org consortium. *Computational Materials Science*, 93:178 – 192, 2014. ISSN 0927-0256. doi:<https://doi.org/10.1016/j.commatsci.2014.05.014>. URL <http://www.sciencedirect.com/science/article/pii/S0927025614003322>.

TABLES

TABLE I: Bulk properties of TiO₂ anatase. a and c are the cell parameters of the tetragonal cell, E_g is the fundamental gap, ϵ_{VV}^∞ and ϵ_{VV}^0 are the symmetry-independent components of the (static) electronic and ionic contributions, respectively, of the dielectric tensor. $\Delta\epsilon_V$ is the offset of the valence band maximum with respect to the value calculated for HSE15. A negative sign means that the HSE15 valence band maximum lies deeper than the valence band of the considered functional.

Property	PBEsol	PBE+ U [Ti]	PBE+ U [Ti,O]	HSE15	Exp.
a (Å)	3.77	3.88	3.86	3.78	3.79[?]]
c (Å)	9.56	9.77	9.74	9.64	9.54 ^a
E_g (eV)	2.08	2.79	2.95	3.12	3.2[?]]
ϵ_{xx}^∞	6.90	5.64	5.42		5.82[?]]
ϵ_{zz}^∞	6.32	5.48	5.30		5.41 ^c
ϵ_{xx}^0	50.88	18.98	17.68		45.1 ^c
ϵ_{zz}^0	22.93	12.62	12.00		22.7 ^c
$\Delta\epsilon_V$ (eV)	-0.70	-0.78	-0.64	0	

TABLE II: Classes of point defects calculated with a given computational approach. \times indicates that the given class of point defects was considered in all specified charge states. The charge states taken into account are: -2,-1,0,+1,+2 for O_{*i*}, 0,+1,+2,+3,+4 for Ti_{*i*}, 0,+1,+2 for □_O, 0,-1,-2,-3,-4 for O_{Ti}, 0,+1,+2,+3,+4 for Ti_O and -1 for the polaron

Defect	PBEsol	PBE+ U [Ti]	PBE+ U [Ti,O]	HSE15
O _{<i>i</i>}	\times	\times	\times	
Ti _{<i>i</i>}	\times	\times	\times	\times
□ _O	\times	\times	\times	\times
□ _{Ti}	\times	\times	\times	\times
O _{Ti}		\times	\times	
Ti _O		\times		
polaron		\times		

TABLE III: Thermodynamic charge transition levels calculated after having aligned the valence band maximum to an unique reference (HSE15 top of the valence band). Values are in eV. A hyphen indicates that the charge transition level is predicted to not exist for the corresponding computational scheme. Transition levels appearing above the experimental band gap of 3.2 eV plus a small tolerance of 0.1 eV are excluded from the table except for comparing with another functional. In this case the values are shown in parenthesis.

Defect	q/q'	PBEsol	PBE+ U [Ti]	PBE+ U [Ti,O]	HSE15
Ti_i	0/1	3.29	(4.00)	(4.02)	(3.40)
	1/3	-	2.73	2.72	-
	1/2	3.19	-	-	3.06
	2/3	3.06	-	-	3.05
	3/4	2.92	2.24	2.19	2.99
\square_{O}	0/1	3.30	2.90	2.91	-
	1/2	2.99	2.70	2.69	-
	0/2	-	-	-	3.25
\square_{Ti}	-1/0	0.73	0.85	-	0.16
	-2/0	-	-	1.18	-
	-2/-1	0.90	1.19	-	0.41
	-3/-2	0.92	1.26	-	-
	-4/-3	0.96	1.48	-	-
	-4/-2	-	-	2.03	0.87

TABLE IV: Formation enthalpies of selected oxides of titanium calculated with different computational setups. In the “PBEsol” column values are obtained by calculating the electronic energies of all species using the PBEsol functional. In the “PBE+ U [Ti]” column, values are obtained by calculating the electronic energy with the PBE+ U [Ti] setup for all compounds except TiO, Ti and O₂, for which PBE was used. In the “PBE+ U [Ti] Corrected” column we apply the correction for the elements as detailed in the main text. All values are reported in eV per formula unit. Note that for the PBE+ U scheme the table reports the antiferromagnetic phase of Ti₂O₃, which is predicted to be the ground-state by this framework. Experimental values represent the formation enthalpies at room temperature and standard pressure. Computed values report the ground-state zero-temperature and zero-pressure values. The last row reports the calculated mean absolute error from the experimental data.

Comp.	PBEsol	PBE+ U [Ti]	PBE+ U [Ti] Corrected	Exp.[?]
Anatase	-9.53	-5.46	-9.73	-9.73
Rutile	-9.47	-5.45	-9.73	-9.79
Ti ₂ O ₃	-15.26	-8.21	-16.09	-15.76
Ti ₃ O ₅	-24.89	-13.47	-25.62	-25.49
TiO	-5.39	-4.62	-5.30	-5.58
MAE	0.36	6.13	0.14	0

TABLE V: Chemical potential values for Ti and O calculated with different methods when O₂ and Ti₂O₃ are the competing phases in O-rich and Ti-rich conditions, respectively. Values in the Exp. column are obtained from the experimental formation enthalpies reported in Table IV.

$\Delta\mu$	(eV)	PBEsol	PBE+ U [Ti] Corrected	HSE06[?]	Exp.
$\Delta\mu_{\text{Ti}}$	O-rich	-9.53	-9.73	-9.76	-9.73
	Ti-rich	-1.92	-2.97	-1.72	-2.34
$\Delta\mu_{\text{O}}$	O-rich	0	0	0	0
	Ti-rich	-3.80	-3.38	-4.02	-3.70

FIGURE CAPTIONS

FIG. 1. O_{Ti} (top) and Ti_{O} (bottom) antisites in the neutral and fully ionized states. The empty square box represents the oxygen vacancy left by the Ti atom after the Ti_{O} defect relaxes. Oxygen atoms are represented in red. The picture was produced using the VESTA software [51].

FIG. 2. Graphical representation of the thermodynamic charge transition levels predicted by the four xc functionals employed in this study for Ti_i , \square_{O} and \square_{Ti} . The lines are obtained from the defect formation energies, whose values have been rigidly shifted for a more clear visualization of the transition levels. The zero of E_F has been set at ϵ_V of HSE15 and valence band maxima have been aligned for all functionals, as explained in the text. Shaded areas show the band edges one would obtain without having aligned the valence band maxima.

FIG. 3. Electronic charge density projected of the levels induced by the neutral \square_{O} defect: (a) PBEsol, (b) PBE+ $U[\text{Ti}]$, (c) HSE15. Isosurfaces level is shown at $0.005 \text{ e}/\text{\AA}^3$. The square represents the position of the oxygen vacancy. Oxygen atoms are shown in red. The plane of the figure is defined by the **b** and **c** cell vectors of the tetragonal cell.

FIG. 4. Electronic charge density projected on the defective levels induced by the fully ionized $(-4) \square_{\text{Ti}}$ defect : (a) PBEsol, (b) PBE+ $U[\text{Ti}]$, (c) HSE15. Isosurfaces level is shown at $0.005 \text{ e}/\text{\AA}^3$. The square represents the position of the titanium vacancy. Oxygen atoms are shown in red. The plane of the figure is defined by the **b** and **c** cell vectors of the conventional tetragonal cell.

FIG. 5. Convex hull calculated in the corrected PBE+ $U[\text{Ti}]$ setup. The red dots represent compounds that lie on the hull or have a distance from it within 25meV/atom. Note that the Ti_2O_3 system on the hull has the antiferromagnetic state; while the non-magnetic one has higher formation energy.

FIG. 6. Comparison between the formation energies of point defects in different charge states for O-rich conditions between: (a) PBEsol and corrected PBE+ $U[\text{Ti}]$ (PBE+ $U[\text{Ti}]$ +C), (b) HSE15

and PBE+ U [Ti]+C, (c) HSE15 and PBEsol, (d) PBE+ U [Ti]+C and PBE+ U [Ti]+C where the cell parameter has been fixed to the PBEsol value (cell 2). The bold black line indicates the ideal case where both schemes give the same formation energies. The dashed line is obtained from linear regression.

FIGURES

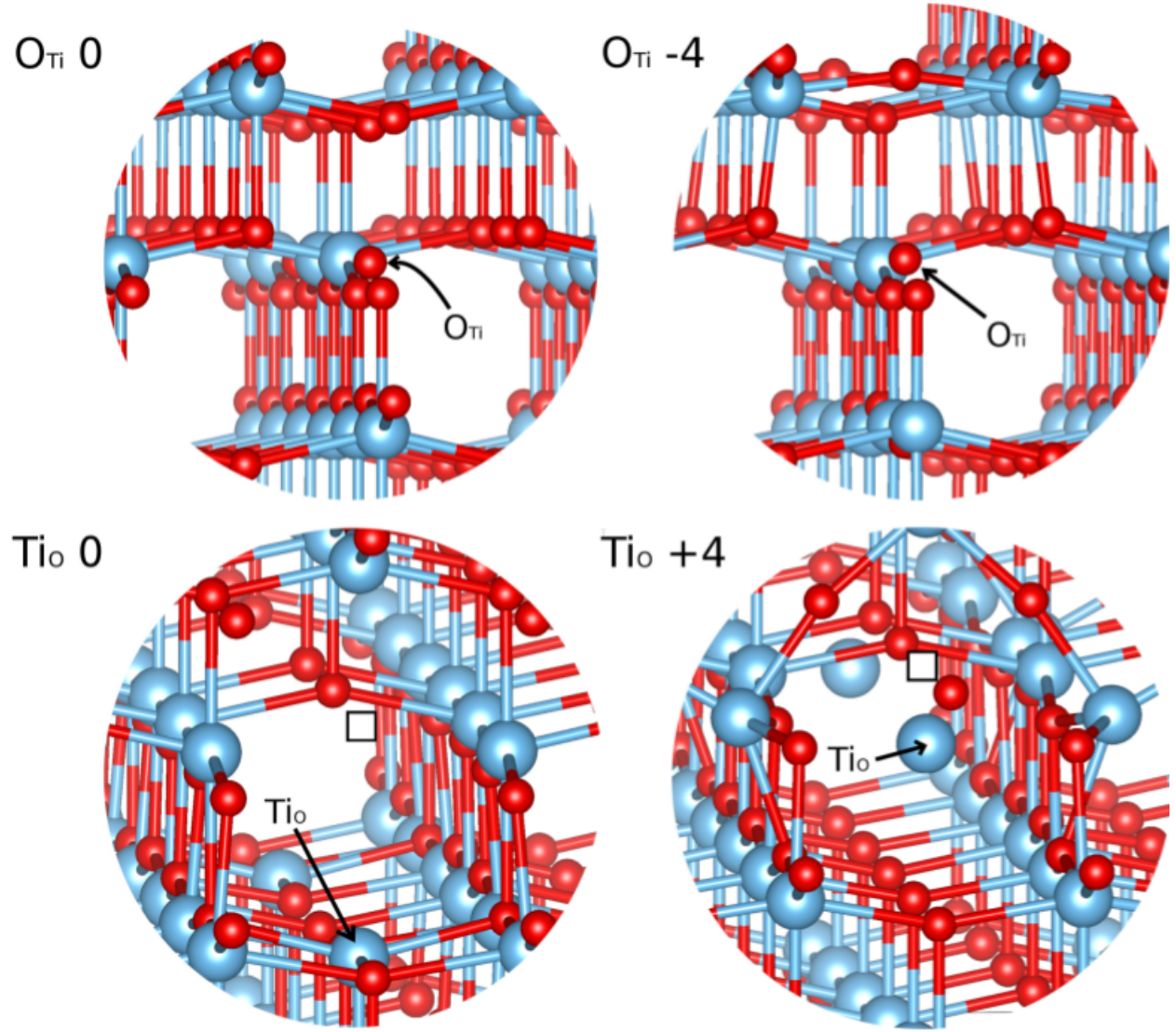


FIG. 1: O_{Ti} (top) and Ti_O (bottom) antisites in the neutral and fully ionized states. The empty square box represents the oxygen vacancy left by the Ti atom after the Ti_O defect relaxes. Oxygen atoms are represented in red. The picture was produced using the VESTA software [51].

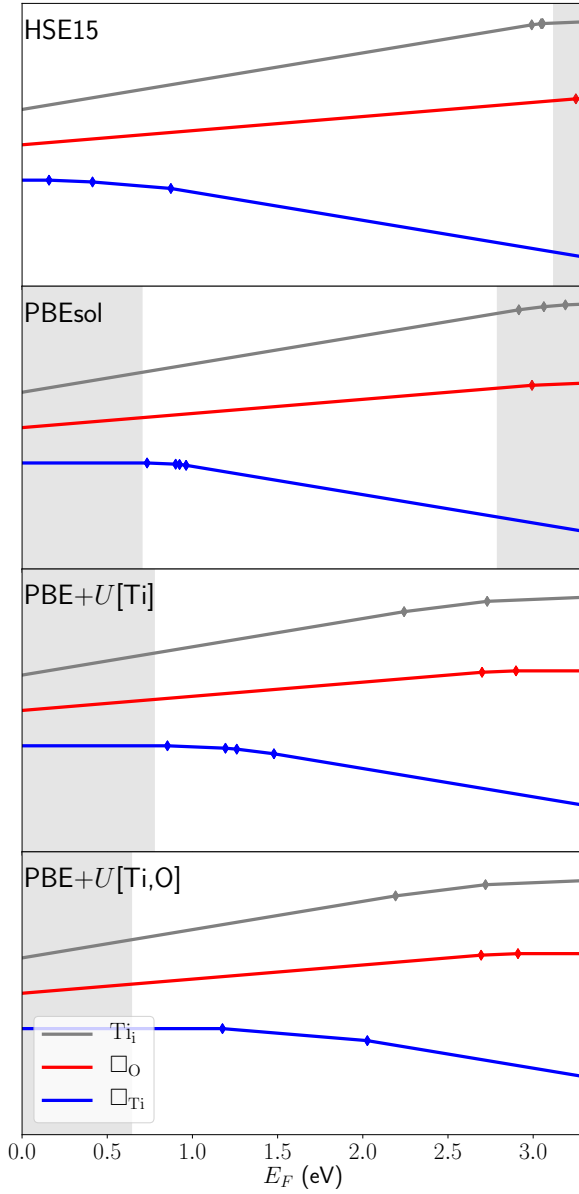


FIG. 2: Graphical representation of the thermodynamic charge transition levels predicted by the four xc functionals employed in this study for Ti_i , \square_{O} and \square_{Ti} . The lines are obtained from the defect formation energies, whose values have been rigidly shifted for a more clear visualization of the transition levels. The zero of E_F has been set at ϵ_V of HSE15 and valence band maxima have been aligned for all functionals, as explained in the text. Shaded areas show the band edges one would obtain without having aligned the valence band maxima.

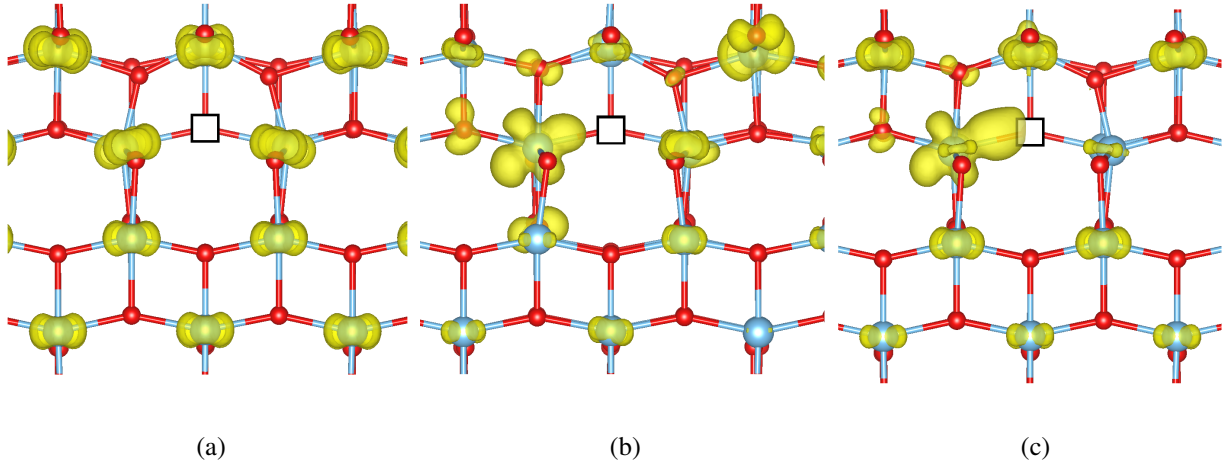


FIG. 3: Electronic charge density projected of the levels induced by the neutral \square_{O} defect: (a) PBEsol, (b) PBE+ $U[\text{Ti}]$, (c) HSE15. Isosurfaces level is shown at $0.005 \text{ e}/\text{\AA}^3$. The square represents the position of the oxygen vacancy. Oxygen atoms are shown in red. The plane of the figure is defined by the **b** and **c** cell vectors of the tetragonal cell.

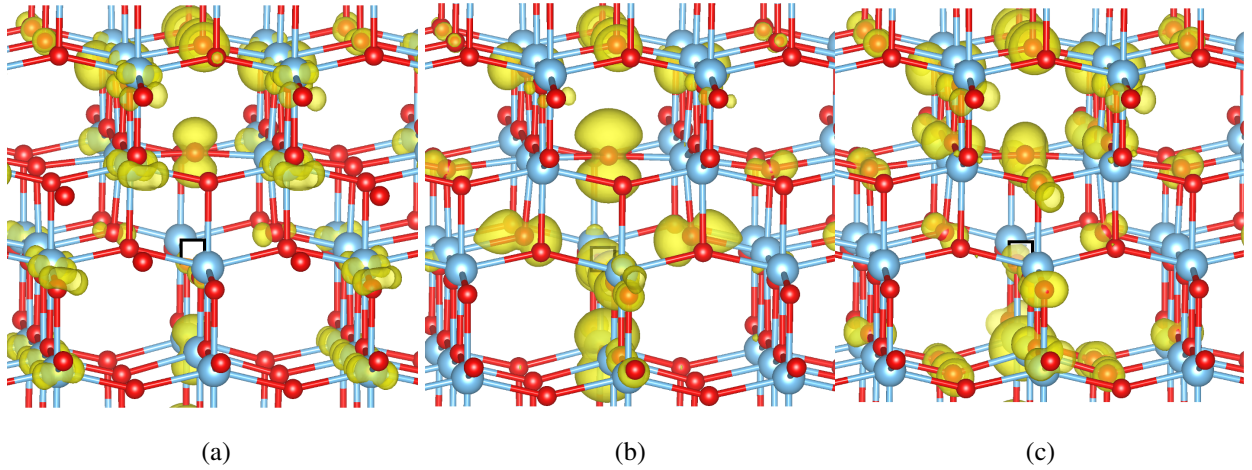


FIG. 4: Electronic charge density projected on the defective levels induced by the fully ionized $(-4) \square_{\text{Ti}}$ defect : (a) PBEsol, (b) PBE+ $U[\text{Ti}]$, (c) HSE15. Isosurfaces level is shown at $0.005 \text{ e}/\text{\AA}^3$. The square represents the position of the titanium vacancy. Oxygen atoms are shown in red. The plane of the figure is defined by the **b** and **c** cell vectors of the conventional tetragonal cell.

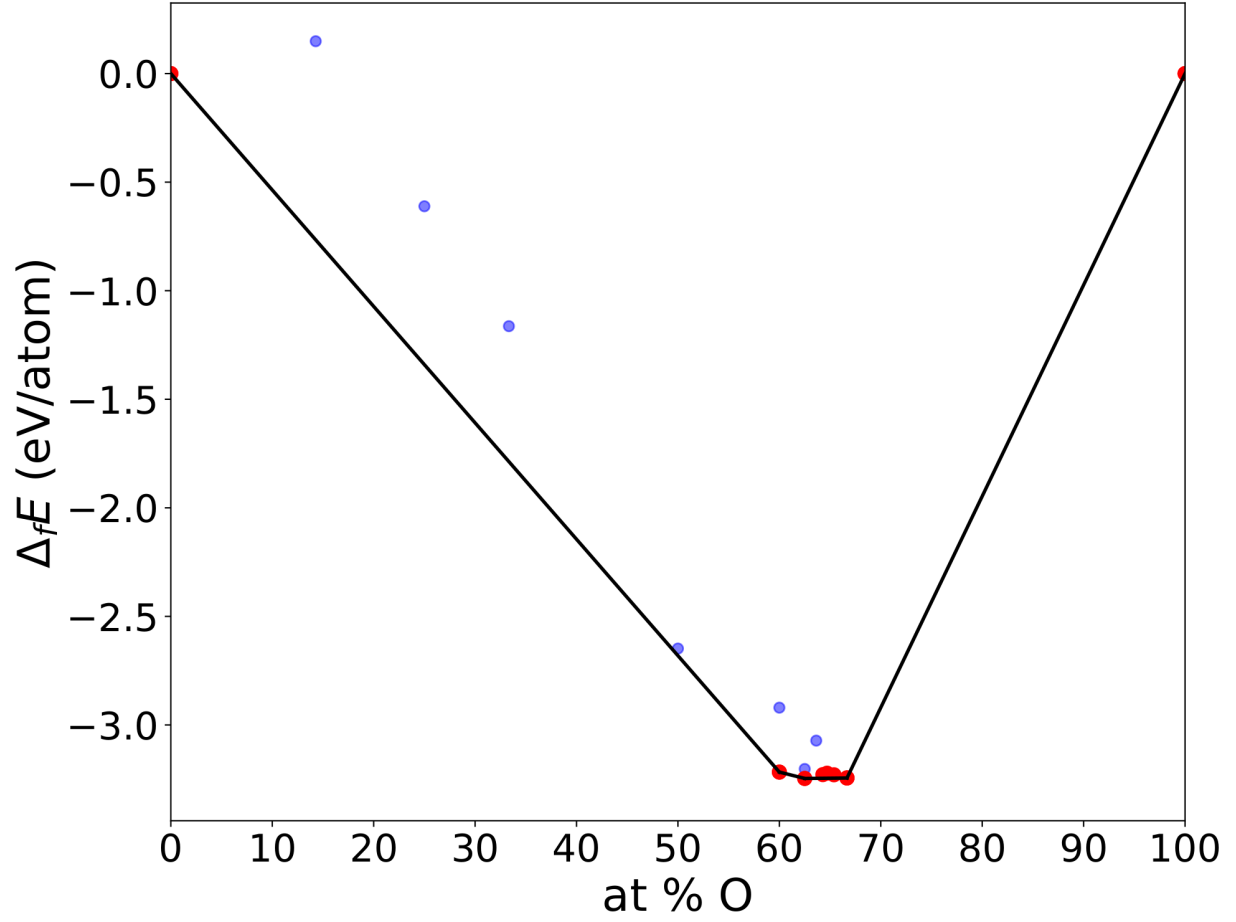
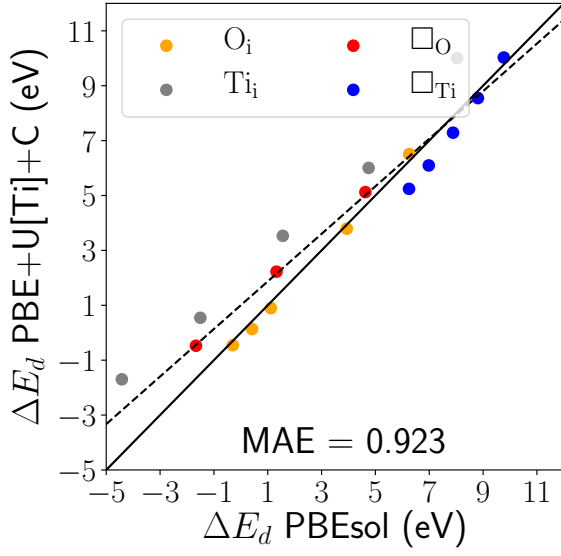
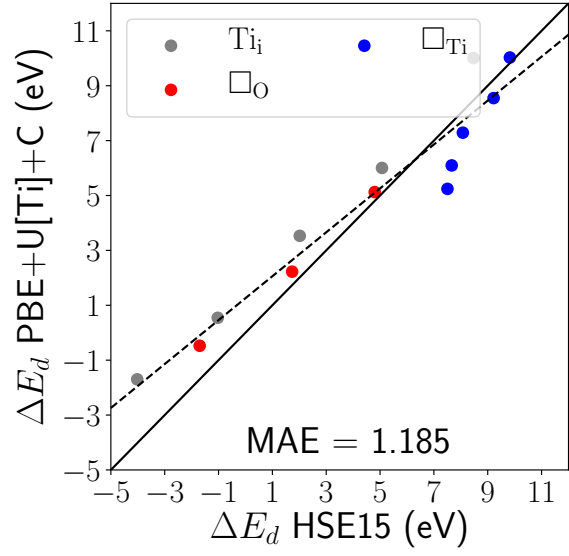


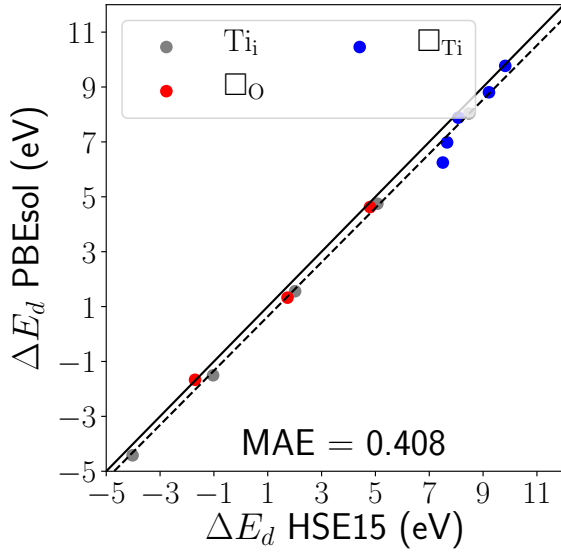
FIG. 5: Convex hull calculated in the corrected PBE+ U [Ti] setup. The red dots represent compounds that lie on the hull or have a distance from it within 25 meV/atom. Note that the Ti_2O_3 system on the hull has the antiferromagnetic state; while the non-magnetic one has higher formation energy.



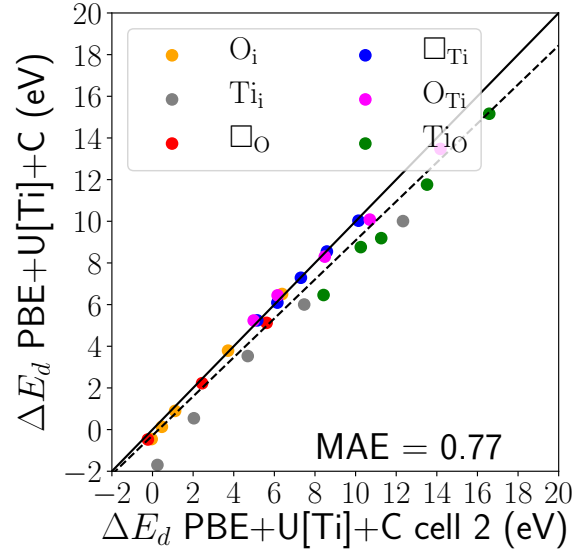
(a)



(b)



(c)



(d)

FIG. 6: Comparison between the formation energies of point defects in different charge states for O-rich conditions between: (a) PBEsol and corrected PBE+U[Ti] (PBE+U[Ti]+C), (b) HSE15 and PBE+U[Ti]+C, (c) HSE15 and PBEsol, (d) PBE+U[Ti]+C and PBE+U[Ti]+C where the cell parameter has been fixed to the PBEsol value (cell 2). The bold black line indicates the ideal case where both schemes give the same formation energies. The dashed line is obtained from linear regression.